

# Low-Loss, Extreme Subdiffraction Photon Confinement via Silicon Carbide Localized Surface Phonon Polariton Resonators

Joshua D. Caldwell,<sup>\*,†</sup> Orest J. Glembocki,<sup>†</sup> Yan Francescato,<sup>‡</sup> Nicholas Sharac,<sup>#,||</sup> Vincenzo Giannini,<sup>‡</sup> Francisco J. Bezares,<sup>†,||</sup> James P. Long,<sup>†</sup> Jeffrey C. Owrutsky,<sup>†</sup> Igor Vurgaftman,<sup>†</sup> Joseph G. Tischler,<sup>†</sup> Virginia D. Wheeler,<sup>†</sup> Nabil D. Bassim,<sup>†</sup> Loretta M. Shirey,<sup>†</sup> Richard Kasica,<sup>§</sup> and Stefan A. Maier<sup>‡</sup>

<sup>†</sup>U.S. Naval Research Laboratory, Washington, DC, United States

<sup>‡</sup>The Blackett Laboratory, Department of Physics, Imperial College London, London, United Kingdom

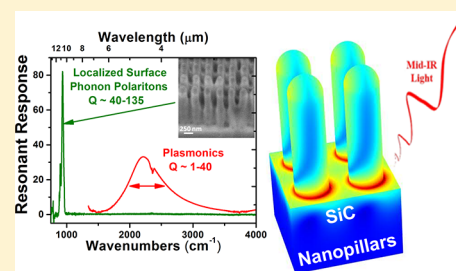
<sup>§</sup>Center for Nanoscale Technology, National Institutes of Standards and Technology, Gaithersburg, Maryland, United States

<sup>#</sup>Chemical Engineering and Materials Science Department, University of California – Irvine, Irvine, California, United States

## Supporting Information

**ABSTRACT:** Plasmonics provides great promise for nanophotonic applications. However, the high optical losses inherent in metal-based plasmonic systems have limited progress. Thus, it is critical to identify alternative low-loss materials. One alternative is polar dielectrics that support surface phonon polariton (SPhP) modes, where the confinement of infrared light is aided by optical phonons. Using fabricated 6H-silicon carbide nanopillar antenna arrays, we report on the observation of subdiffraction, localized SPhP resonances. They exhibit a dipolar resonance transverse to the nanopillar axis and a monopolar resonance associated with the longitudinal axis dependent upon the SiC substrate. Both exhibit exceptionally narrow linewidths (7–24 cm<sup>-1</sup>), with quality factors of 40–135, which exceed the theoretical limit of plasmonic systems, with extreme subwavelength confinement of  $(\lambda_{\text{res}}^3/V_{\text{eff}})^{1/3} = 50\text{--}200$ . Under certain conditions, the modes are Raman-active, enabling their study in the visible spectral range. These observations promise to reinvent research in SPhP phenomena and their use for nanophotonic applications.

**KEYWORDS:** Optical phonon, polar dielectric, phonon polariton, silicon carbide, nanopillar, subdiffraction confinement, plasmonics, nanoantenna, mid-infrared



Once the seminal work of Ritchie<sup>1</sup> on surface plasmon polaritons (SPPs) in thin metallic foils was extended to local surface plasmon resonators, the realization that optical confinement was no longer limited by the Abbe diffraction limit helped launch the field of plasmonics. The subdiffraction confinement of light has enabled the fields of nanophotonics,<sup>2,3</sup> metamaterials,<sup>4,5</sup> and enhanced molecular spectroscopy using techniques such as SERS<sup>6</sup> (surface-enhanced Raman scattering) and SEIRA<sup>7–9</sup> (surface-enhanced IR absorption). Unfortunately, while a great deal of progress has been made, achieving the full promise of plasmonics is hampered by the short lifetimes of plasmons associated with electrons in metals at optical wavelengths (~tens of femtoseconds), resulting in high optical losses.<sup>10</sup> In recent years, efforts have focused on identifying potential lower-loss plasmonic materials<sup>11,12</sup> with particular attention paid to transparent conductive oxides<sup>13</sup> and, more recently, graphene.<sup>14–16</sup> However, these materials still require free carriers (electrons and/or holes) to support the localized electromagnetic fields and thus remain prone to losses due to the associated fast plasmon decay.

The subdiffraction confinement of light can also be achieved through the stimulation of *surface phonon polaritons* (SPhPs) within polar dielectrics, such as SiC,<sup>17</sup> III-Ns,<sup>18</sup> III-Vs,<sup>19</sup> and SiO<sub>2</sub>.<sup>20,21</sup> SPhP excitations achieve optical confinement in the

mid-IR to terahertz range through the coherent oscillation of the charged atomic species on a polar lattice (optical phonons) within the so-called Reststrahlen band, where the permittivity is negative. The relevant optical phonons exhibit picosecond lifetimes, which are orders of magnitude longer than the scattering times of free carriers that support surface plasmon modes in metals and doped semiconductors.<sup>22</sup> Even taking into account the relatively low oscillation frequencies of optical phonons, the ratio of the resonant frequency to the damping rate is nearly an order of magnitude larger than in any plasmonic system reported to date. This results in a material system exhibiting exceptionally low optical losses. Similar to plasmonic systems, the SPhP oscillation is expected to become highly localized within confined geometries.<sup>22</sup> Initial explorations into SPhP modes were reported in the seminal work of Mutschke et al.,<sup>23</sup> where the infrared spectral properties of various SiC grains and particles were explored in an effort to understand spectral features of such particulates within carbon-rich stars, and of Hillenbrand et al.,<sup>17</sup> where scattering near-field optical microscopy (s-SNOM) measurements of silicon carbide

Received: May 1, 2013

Revised: June 26, 2013

Published: July 1, 2013



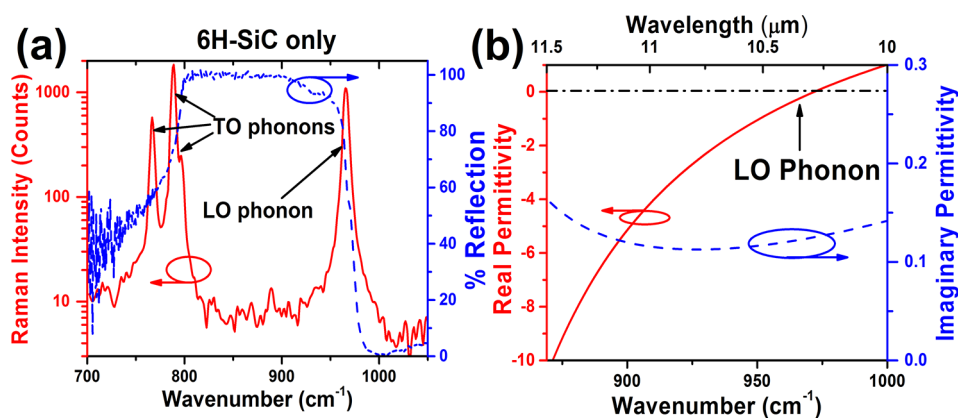


**Figure 1.** (a) Micro-Raman (red solid line) and FTIR reflection (blue dashed line) spectra of a 6H-SiC substrate, illustrating the role of the LO and TO phonons in defining the highly reflective Reststrahlen band. (b) Real and imaginary parts of the permittivity determined from fitting of the reflection spectra of the 6H-SiC substrate used for nanopillar fabrication. The spectral range provided coincides with that of the position of the LO phonon and the observed localized SPhP modes presented in this work. A horizontal dashed/dotted line corresponds to the real permittivity equal to zero.

surfaces were employed. In the latter work, the image charge of a platinum-coated s-SNOM tip in the SiC substrate imitated the behavior of a localized SPhP resonance. Anderson<sup>7</sup> later used SiC and Al<sub>2</sub>O<sub>3</sub> spherical particles to explore the potential for SPhP materials for SEIRA applications, reporting enhancements in excess of 100×. Later work by Schuller et al.<sup>24</sup> demonstrated both broad dielectric resonance modes as well as a SPhP resonance at wavelengths within the Reststrahlen band that are supported by high-aspect-ratio SiC wires with diameters of 1–3 μm. These experiments, together with the studies of polar dielectrics utilized for SPhP-based mid-IR superlensing,<sup>25</sup> SPhP propagation<sup>26,27</sup> and focusing,<sup>28</sup> sub-wavelength extraordinary transmission gratings,<sup>29</sup> and IR thermal emitting meta-surfaces<sup>24,30,31</sup> have demonstrated the promise of these materials. Furthermore, recent advances in the material quality of SiC have dramatically reduced the optical losses in semi-insulating substrates and epitaxial layers due to reductions in the extended and point defect densities and improvements in the growth processes.<sup>32,33</sup> However, user-defined, fabricated SPhP nanostructures are crucial for the development of *localized* resonators for optical antennas and enhanced molecular spectroscopy at size scales below those achievable with ordinary dielectric resonators<sup>34</sup> and have not yet been reported experimentally with results being limited to theory.<sup>8,35,36</sup>

Up until the work reported here, efforts to fabricate localized SPhP resonators with defined resonant response were held back by the knowledge that ion implantation via focused ion-beam (FIB) into a SiC surface led to significant damping of the SPhP response in s-SNOM.<sup>37</sup> While in that work the implantation was designed to “turn-off” the SPhP response for the development of patterned SPhP surfaces, this observation also led to the anticipation that the use of standard fabrication processes such as FIB or reactive ion etching (RIE) for nanostructure formation in SiC would lead to similar damping and preclude the observation of localized SPhP modes. Here, we demonstrate the contrary by reporting on the first experimental observations of nanofabricated, localized SPhP resonant modes using standard RIE processing to fabricate periodic arrays of 6H-SiC nanopillars with diameters 40–75× smaller than the incident wavelength ( $D = 150\text{--}260\text{ nm}$ ). The resultant localized resonances exhibit exceptionally narrow linewidths of 7–24 cm<sup>-1</sup>. This corresponds to quality ( $Q$ )-

factors in the range of 40–135, which surpass what is theoretically possible for localized surface plasmons.<sup>10,38–43</sup> These high  $Q$ -factors are coupled with modal volumes  $(\lambda_{\text{res}}^3/V_{\text{eff}})^{1/3}$  of the resonant modes that were calculated to be ~50–200× smaller than the resonant wavelength,  $\lambda_{\text{res}}$ , and predict potential Purcell factors as high as  $F_p = 6.4 \times 10^7$ . Such large values of  $F_p$  imply a dramatic enhancement in the spontaneous emission rates of nearby emitters, which in this spectral range could have significant implications for tailoring the blackbody response<sup>24,31,44</sup> and enhancing the absorption of IR-active vibrational modes for the SEIRA effect.<sup>7–9</sup> For comparison, theoretical work on isolated and near-field coupled silver nanospheres predict potential Purcell factors up to 1000,<sup>45</sup> and even with the highest theoretically possible plasmonic  $Q$ -factors<sup>10</sup> the Purcell factors still do not exceed 10.<sup>4</sup>

We further show that the transverse and longitudinal resonances anticipated for isolated subwavelength nanorods<sup>22</sup> are transformed by the presence of the underlying SiC substrate into a higher-energy transverse dipolar and a lower-energy monopolar resonance with both modes spectrally shifting with changing nanostructure geometry. The monopolar mode may be thought of as evolving from the longitudinal dipole resonance of a free-standing pillar when the underlying SiC substrate modifies the electric-field symmetry of the mode and can be excited only with off-normal incident light. The extreme subdiffraction confinement also enhances the intensity of the incident electromagnetic field by more than 5000 times, which is essential for coupling to and enhancing optical processes of nearby emitters. Further, we find that under certain conditions, these mid-IR SPhP modes become Raman-active, which enables their study via Raman scattering in the visible spectral range with higher spatial resolution than is available in the mid-IR.

These results demonstrate the potential for a new approach to nanophotonic resonators using localized SPhP modes in polar dielectrics. On the basis of the relatively long lifetimes and low optical loss associated with these phonon-based modes, SPhP excitations in polar dielectrics open the door to exciting possibilities such as the realization of epsilon-near-zero<sup>46</sup> and negative index metamaterials<sup>34</sup> as well as on-chip nanophotonics<sup>47</sup> in the mid- to far-IR regions. These results promise to reinvestigate basic research studies of SPhP modes

within polar dielectric materials and should lead to dramatic advancements in the fields of nanophotonics and metamaterials.

At wavelengths between the longitudinal (LO) and transverse (TO) optical phonon modes, the charged atomic species of a polar lattice can be optically induced to oscillate coherently in the form of SPhPs. Analogous to coherent free carrier oscillations in metals (plasmons), this results in a screening of incident photons through the motion of the underlying charged lattice, which produces a spectral region of high reflectivity that is referred to as the “Reststrahlen” band.<sup>17,22</sup> This phenomenon is visualized in Figure 1a by overlapping the optical phonon energies as revealed by Raman scattering (red solid line) onto the reflection spectrum within the Reststrahlen band (blue dashed line) of the 6H–SiC substrate used for these studies. Within this spectral range, the SiC resembles a metal with the reflectivity approaching 100%. This corresponds with the real part of the permittivity crossing through zero near the LO phonon energy and becoming increasingly negative as the energy is decreased (red, solid line in Figure 1b). This behavior extends to the TO phonon energy at which point the permittivity reaches a minimum before becoming positive once again. It is within this Reststrahlen spectral range that SiC and other polar dielectric nanostructures can support localized SPhP resonant modes that are analogous to those of plasmonic nanostructures.<sup>22</sup> In addition, over much of this range optical losses are low as illustrated by the small imaginary part of the permittivity (blue dashed line in Figure 1b).

In order to explore the possibility of inducing localized SPhP resonant modes and to identify their characteristics, we fabricated a series of periodic arrays of 6H–SiC nanopillars with diameters varying between 150 and 260 nm. Doing so enables comparisons with plasmonic nanostructures to identify if the formalisms are directly analogous, as was anticipated by Bohren and Huffman.<sup>22</sup> To reduce the presence of residual surface-bound fluorine and surface damage induced by the RIE process used for fabrication, a subsequent etch in H<sub>2</sub> gas at 1400 °C was employed, which rounded the top of the cylindrical nanopillars and resulted in some variability in the nanopillar shape (SEM in inset of Figure 2), while reducing the SPhP resonance line width by a factor of 2–4×. Presented in Figure 2 is the IR reflection spectrum from the 6H–SiC substrate (green dashed line) and the same substrate with a periodic array of 800 nm tall, 250 nm diameter nanopillars (red solid line) on a pitch of 400 nm (interpillar gap of 150 nm). The nanostructure fabrication resulted in the observation of two primary localized SPhP resonant modes that provide for low-albedo surfaces that are useful for resonant spectral response. These localized SPhP absorption peaks are superimposed upon the broad, highly reflective Reststrahlen band and in many cases exceed 90% extinction. These are similar to the resonances observed by Urzhumov et al.<sup>29</sup> within extraordinary transmission gratings of 1–2 μm diameter holes in 3C–SiC membranes. The additional two modes observed near 882 and 888 cm<sup>-1</sup> can be attributed to a splitting of a doubly degenerate, axial bulk optical phonon (2A<sub>1</sub> symmetry), and while only observed in the IR reflection spectra from the nanopillar arrays, they are not due to localized SPhP modes.<sup>48</sup> Since these modes are not observed within the surrounding unpatterned substrate, they are not incorporated within the derived optical constants and not observed within the simulated spectra in Figure 2.

In order to understand the localized SPhP modes in greater depth, we modeled the local electromagnetic fields by

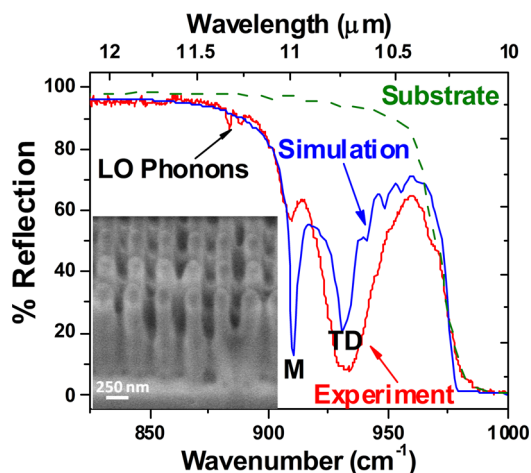


**Figure 2.** FTIR reflectance spectrum of a periodic array of 250 nm diameter, 6H–SiC nanopillars (red solid line) on a 400 nm pitch compared to a COMSOL-simulated spectrum (blue solid line). “M” and “TD” denote the spectral positions of the monopole and transverse dipole resonances, respectively. For comparison, the reflection spectrum of the surrounding 6H–SiC substrate is also provided (dashed green line). An SEM image collected at 45° is provided in the inset.

numerically solving Maxwell’s equations with the COMSOL Multiphysics software. Also presented in Figure 2 is the calculated reflectance spectrum (blue solid line) for a 6H–SiC substrate patterned with nanopillars matching those from the experiment. The calculated spectra reproduce the two modes well. It was experimentally observed that the higher-energy resonance varied with the nanopillar diameter and was only weakly dependent on the incidence angle and interpillar gap. These observations along with the calculated cross-sectional and top-view electromagnetic field profiles depict this as a dipolar, transverse resonance, analogous to modes observed in plasmonic nanorods (Figure 3a,c, respectively; see also Figures S4 and S5 in the Supporting Information).<sup>22</sup> The second, lower-energy resonance was observed experimentally to be strongly dependent upon the nanopillar diameter and interpillar gap and to increase in intensity at larger incident angles. This dependence on interparticle gap is likely due to interpillar coupling, as discussed in depth in the literature,<sup>42,49</sup> and will be the subject of subsequent work. Modeling of this mode determined that it can only be stimulated with off-normal excitation. This behavior is supportive of its identification as a longitudinal mode, as is expected for isolated nanorods. However, the simulations (Figure 3b) demonstrate a significant concentration of the electric field near the base of the nanopillar, which is not characteristic of a longitudinal dipole mode. The plan-view  $E_z/E_0$  profile calculated for a plane just below the substrate surface (Figure 3d), indicates that this mode is instead a lower-order, monopolar resonance. While monopoles cannot be excited in isolated nanopillars, charge-neutrality in this case is achieved by the opposing field located near the surface of the SiC substrate in the region between the nanopillars. For comparison, subdiffraction monopole resonances have been recently reported in plasmonic nanorods with metal ground planes,<sup>50,51</sup> similar to an RF monopole antenna. In the case described here, additional simulations imply that the monopole resonance originates from a modified longitudinal mode and that expanding the periodicity of the array enables the observation of higher-order monopole resonance modes,

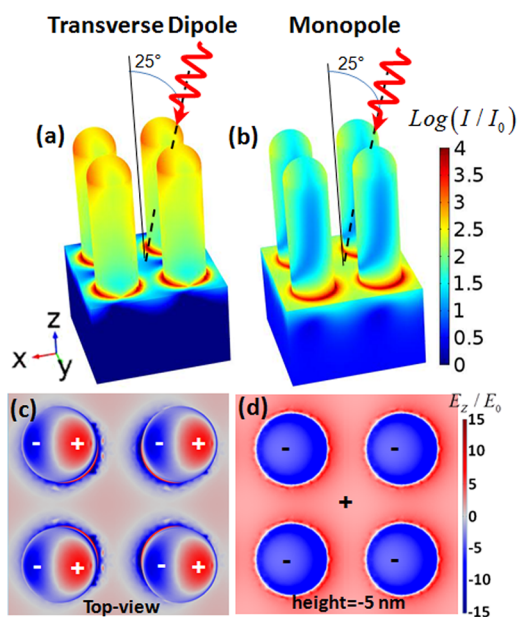


**Figure 3.** Calculated electromagnetic intensity profiles,  $\log(I/I_0)$  for the (a) transverse dipolar and (b) monopolar modes. The corresponding top-view electromagnetic field profile ( $E_z/E_0$ ) of the (c) transverse dipolar mode and the corresponding plan-view profile of the (d) monopolar mode at 5 nm below the substrate surface (to avoid interface effects and to clearly depict the role of the substrate). In all cases, the incident plane wave in the calculations was directed toward the sample at  $25^\circ$  off normal from right to left, as depicted by the schematic in (a) and (b).

similar to the modes of nanorod plasmonic antennas<sup>50,51</sup> on conductive substrates. The calculated spatial profiles of the local SPhP fields for the transverse dipolar and monopolar resonances indicate that these modes provide deeply subwavelength field confinements of approximately  $(\lambda_{\text{res}}^3/V_{\text{eff}})^{1/3} = 50\text{--}200$  with values of 115 and 199 calculated for the transverse dipolar and monopolar modes, respectively, within an array of 250 nm diameter nanopillars on a 400 nm pitch. As illustrated by the logarithmic plots of the electric field intensities presented in Figure 3a,b, enhancements well in excess of 5000 $\times$  are predicted by these simulations (maximum intensities of 27 700 and 15 700 were calculated for the transverse dipole and monopole modes, respectively). These enhanced local fields are positioned on the surface of the nanostructure and for the most part are excluded from the volume of the nanopillar. This is similar to the surface fields in localized surface plasmon structures and is important for downstream applications, where only those fields outside of the nanostructure volume can be harnessed for enhancing optical processes in nanoscale emitters or molecular vibrational signatures. On the other hand, owing to the strong dispersion of SiC in this spectral range, the electric energy density is larger inside the pillar.

As in the case of any damped oscillator, the ratio between the resonant frequency and the resonance line width  $\omega_{\text{res}}/\Delta\omega_{\text{res}}^{\text{fwhm}}$ , or quality factor  $Q$ , represents the rate of energy lost with respect to the stored energy within the resonator. The measured  $Q$ -factors for the transverse dipole and monopole resonances within this sample set ranged from 40 to 50 and 70 to 135, respectively. As stated above, these experimental results exceed values reported for single plasmonic nanoparticles with silver having a theoretical limit of about 40,<sup>10</sup> as well as a value

previously reported for a SPhP mode in SiC nanowires,<sup>24</sup> where a  $Q$ -factor value of 16 was reported for  $\text{TE}_{\pm 1}$  mode, which can be compared to the transverse dipolar resonant mode discussed in this work. Our results are also consistent with ongoing work performed independently by Wang et al.<sup>52</sup> in which s-SNOM measurements find  $Q$ -factors of 50–65 for SPhP resonances inside of holes fabricated in a gold film on top of a SiC substrate. These experimental  $Q$ -factors are by no means the upper limit for what can be realized in these systems. Instead, calculations based on optical constants derived from ellipsometry measurements of SiC epitaxial layers predict  $Q$ -factors in excess of 250. Further, the variable sizes of the nanopillars within any given array likely contributed to a reduction of the apparent  $Q$ -factor from such theoretical values, although further work to separate the effect of surface damage from other inhomogeneities is needed. While the  $Q$ -factor provides a good figure of merit, it does not consider the modal volume, and hence does not incorporate the confinement of the electromagnetic energy. This latter point is especially important for the development of resonators for nanophotonic applications, which exclude wavelength-scale or larger resonators such as photonic crystals or whispering-gallery resonators. In order to compare nanophotonic structures of different sizes, shapes, and frequencies that result from different optical phenomena (e.g., plasmonic, SPhP, or dielectric cavity), we can employ the Purcell factor, defined as  $F_p = [3/(4\pi^2)](\lambda_{\text{res}}/n)^3(Q/V_{\text{eff}})$  with  $V_{\text{eff}}$ ,  $\lambda_{\text{res}}$ , and  $n$  denoting the effective modal volume,<sup>53</sup> the resonant wavelength, and the refractive index of the ambient, respectively. Using the experimental linewidths and the modal volumes calculated for these nanostructures, it was determined that on average the transverse dipole and monopole resonances within the arrays studied exhibit potential Purcell factors of  $F_p = 4.8 \times 10^6$  and  $5.2 \times 10^7$ , respectively, which are lower only by a factor of 2.5–5 $\times$  within the ambient. By incorporating the theoretical linewidths for these modes (6.5 and 4.8  $\text{cm}^{-1}$ ), the  $F_p$  values for such structures are estimated at approximately  $1.6 \times 10^7$  and  $1.3 \times 10^8$ . To our knowledge, these are the highest reported experimental and theoretical  $F_p$  for nanoscale resonators, exceeding the best reported values for even plasmonic/dielectric hybrid resonators by at least an order of magnitude<sup>38,39,54,55</sup> with these systems designed to limit optical losses by confining the fields within the low-loss dielectric regions. Yet the results reported here were achieved without any design optimization. Such large values of  $F_p$  imply the potential for such localized SPhP resonators for modifying the thermal blackbody emission and nearby emitters (molecular vibrational modes or potentially quantum emitters).

By analogy with subwavelength plasmonic nanorods, varying the diameter of these 6H-SiC nanopillars modifies the resonance spectral position while maintaining a fairly constant line width. For the transverse dipole mode, we observed about 4% variation in the line width over the range of diameters investigated (150–260 nm) for a constant interpillar gap of  $\sim 150$  nm. This relative insensitivity of line width to nanopillar size is presumably due to the short mean-free-path of the optical phonons, which reduces the importance of boundary scattering. In contrast, plasmonic systems are susceptible to boundary-scattering losses because of large free-carrier mean-free paths. The short mean-free path of these long-lived, optical phonons are due to their slow group velocity and inherently leads to lower scattering and thus enables the longer lifetimes and low optical losses associated with these modes to be

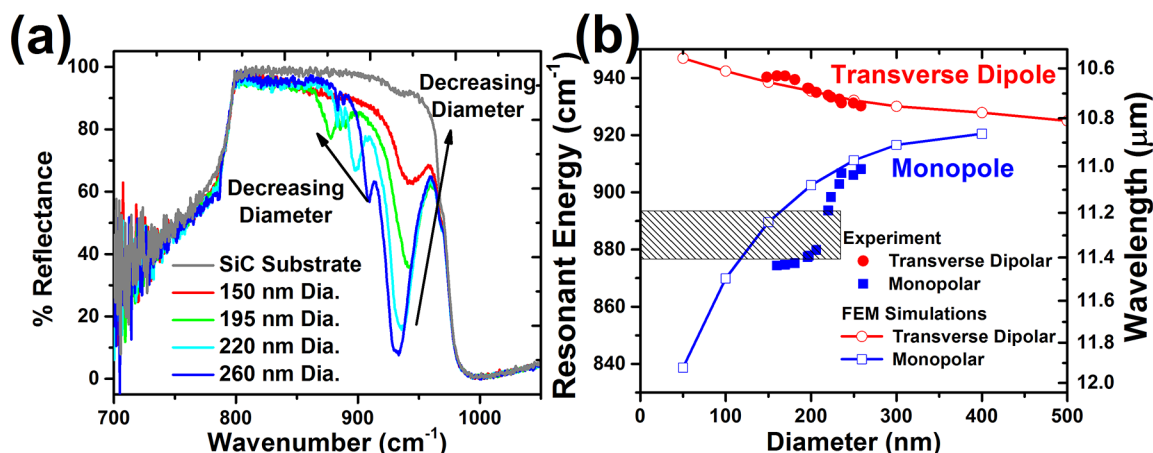


**Figure 4.** (a) FTIR reflection spectra of 800 nm tall, 6H-SiC nanopillars as a function of diameter and for the unpatterned substrate. The arrows designate the direction of the peak shifts for the two modes with decreasing diameter. (b) Corresponding peak positions for the two modes (red circles and blue squares) as a function of diameter in comparison to the computed values using the COMSOL software (open symbols; lines are a guide to the eye). The cross-hatched area corresponds to the spectral region where the monopolar resonance shifts through the peak positions of the LO phonons as discussed in the text.

maintained even within nanostructures on the nanometer-scale and underpins the promise of the SPhP phenomena.

Similar to their plasmonic counterparts, the localized SPhP resonances were observed to shift with changing nanopillar diameter, as shown in Figure 4a. A plot of the corresponding experimental (solid symbols) and calculated (open symbols) spectral position of the transverse dipolar (red symbols) and monopolar (blue symbols) resonances as a function of diameter is presented in Figure 4b. Despite the inevitable complexities associated with structural variations in the experimental nanostructures that are unaccounted for within the COMSOL calculations, the general trends in the diameter dependences of the experimental resonances are semiquantitatively reproduced. However, there are clear deviations between the calculated and experimental spectral positions for the monopolar resonance when the resonance position approaches and crosses the spectral range of  $\sim 878\text{--}892\text{ cm}^{-1}$  (cross-hatched region in Figure 4b; further details in Supporting Information). Within this region, interference between the  $A_1$  (LO) phonon lines and the monopole resonance is observed. This results in a broadening and asymmetry developing within the line shape of the monopole resonance that resembles Fano interference. The Fano effect results from an interference between a discrete optical transition and a much broader continuum mode<sup>56</sup> in this case resulting from the discrete LO phonon modes and the broader monopole SPhP resonance. Similar effects in 4H-SiC nanopillar arrays fabricated in both semi-insulating and highly doped substrates were also observed by our group and will be the subject of a subsequent report. Consequently, this interference effect, while quite interesting, also makes the accurate extraction of the monopolar resonance spectral position problematic and is responsible for the apparent discrepancy between the experiment and theory.

Because the localized SPhP modes observed here are derived from optical phonons, an additional investigation using micro-Raman spectroscopy was undertaken using 532 nm excitation. In many cases, the transverse dipolar and monopolar collective modes were found to be Raman-active. This is demonstrated in Figure 5, which presents both FTIR reflection and micro-Raman spectra collected from a 200 nm diameter nanopillar array (350 nm pitch, 800 nm height). Surface optical phonon

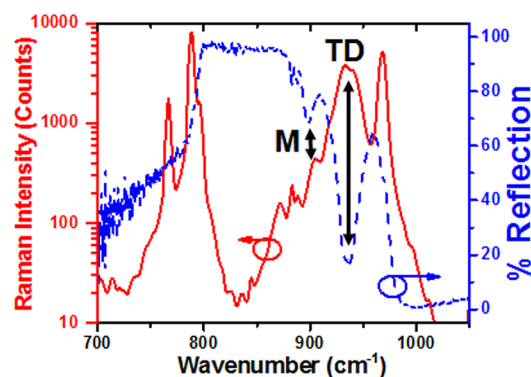


**Figure 5.** FTIR reflection (blue dashed line) and micro-Raman (red solid line) spectra from a periodic array of 6H-SiC nanopillars (200 nm diameter, 800 nm tall, 350 nm pitch). The double-headed arrows correspond to the positions of the two SPhP resonances as labeled.

modes have been observed in Raman spectra for nanowires of various polar dielectric materials<sup>57</sup> but have not been correlated with the localized SPhP phenomenon until now. In all arrays measured, a broad resonance at approximately  $934\text{ cm}^{-1}$  was observed. The localized SPhP resonance modes were observed within the Raman spectra when their resonance position was near the peak position of this aforementioned surface optical mode, implying that their observation is due to a resonant enhancement of the localized SPhP response with these surface optical modes. It should be noted that as the localized SPhP resonances were spectrally shifted away from the surface optical mode, their intensity decreased and in many cases they were no longer observable. In most cases, the surface optical phonon modes and the localized SPhP transverse dipole resonances overlapped, thus it is unclear whether the surface optical mode is observed within the FTIR measurements from the nanopillar arrays. However, a slight dip in the reflection spectra of the bare SiC substrate (Figure 4a) is also observed near  $934\text{ cm}^{-1}$  and may be related to optical phonons confined to the SiC/air surfaces. The direct correlation between these Raman-active modes and the localized SPhP resonances will be explored in more detail in subsequent work. The correlation between these surface optical phonon modes with the localized SPhP

resonances reported here, raises the possibility of using micro-Raman with its submicrometer spot and sensitive detectors unavailable in the mid-IR, to explore single Mie resonators. In addition, one might exploit the resonant electromagnetic field enhancements within these SPhP resonators to enhance Raman spectra from nearby molecules, similar to efforts using dielectric Mie resonators<sup>58</sup> or the SERS effect in plasmonic nanostructures<sup>59</sup> and thus may provide a complementary means to perform enhanced spectroscopy using the same nanostructure.

In summary, we have reported on the experimental observation of localized surface phonon polariton (SPhP) resonances by using nanofabricated, periodic arrays of cylindrical, 800 nm tall, 150–260 nm diameter 6H–SiC nanopillars. This nanostructuring of the SiC substrate induced two localized SPhP resonances, which can be described as transverse dipolar and monopolar resonant modes. The latter results from a modification of the longitudinal dipole resonance due to the underlying SiC substrate. Similar to their plasmonic counterparts, changes in the nanopillar geometry shift the resonances, demonstrating that predictable tuning can be achieved through nanostructure size, shape and selection of polar dielectric material. As the SPhP modes are derived from long-lived optical phonons, they exhibit exceptionally narrow linewidths (fwhm of 7–24  $\text{cm}^{-1}$ ). Such linewidths correspond to quality factors of 40–135, which when coupled to the very small modal volumes of the SPhP modes  $(\lambda_{\text{res}}^3/V_{\text{eff}})^{1/3} \sim 50\text{--}200$ , result in potential Purcell factors between  $1.9 \times 10^6$  and  $6.4 \times 10^7$ . These values well exceed what is theoretically achievable in plasmonic nanoparticles and what has been reported for plasmonic/dielectric hybrid resonators and thus present a glimpse of the potential of localized SPhP modes in polar dielectric materials.

That localized SPhP modes can be stimulated within nanostructures formed via standard lithographic procedures opens up an entirely new approach of employing low-loss, polar dielectrics as an alternative to plasmonics for nanophotonic and metamaterial applications. The observation that these localized SPhP resonances are in many cases Raman-active also enables the study of the modal properties with higher spatial resolution, potentially enabling single-resonator studies. Further, the high field enhancements ( $>5000\times$ ) computed for these SPhP resonators, coupled with their spectral position within an atmospheric transmission window featuring an extensive number of molecular vibrational modes, promise advancements in molecular sensing, both in the lab and at stand-off distances, as well as potentially contributing to the development of components for mid-IR free-space communications. These resonators may also enable improved efficiency and/or reduced pixel-size infrared photodetectors, emitters and imagers. Finally, the inherently long lifetimes (low-loss) and short mean-free paths associated with these resonant modes will provide opportunities to explore the fundamental limits of optical confinement and interparticle coupling that are out of reach for plasmonic nanostructures.

**Methods.** *SiC Nanopillar Fabrication and Characterization.* The silicon carbide nanopillars were fabricated in semi-insulating 6H–silicon carbide substrates approximately 350  $\mu\text{m}$  thick using an Al/Cr hard mask that was defined using standard electron beam lithography, electron beam metal evaporation, and liftoff processes. Nanopillars were fabricated via reactive ion etching (RIE) in equal partial pressures of  $\text{SF}_6$  and Ar at 150 W power and room temperature for 38 min. The metal hard mask

was removed in wet chemical etchants. To remove any surface damage induced via the RIE process and remove any surface-bound fluorine a subsequent surface etch in hydrogen atmosphere was performed in the growth cell of an Aixtron VP508 growth reactor at 1400  $^\circ\text{C}$  for 3 min. Calibration of this process demonstrated that this etch removed approximately 8 nm of SiC surface material. The localized SPhP resonances were characterized using both FTIR and micro-Raman spectroscopy. Mid-IR reflectance measurements were undertaken using a Thermo Scientific, Nicolet FTIR Continuum Microscope with a 15 $\times$ , 0.58 NA objective, which illuminates the sample with a standard glow bar at incident angles between 10 and 35 $^\circ$  off normal with a weighted-average of 25 $^\circ$ . This off-angle excitation enabled excitation of both transverse dipolar and monopolar modes within the nanopillars. The spectra were collected with a 0.5  $\text{cm}^{-1}$  resolution with 128 scans averaged for the final spectra, which were collected from a spatial area defined by the internal aperture that was set to 50  $\times$  50  $\mu\text{m}$ . To improve the signal-to-noise, an initial background reflection spectrum from a gold film was collected at the same spectral resolution but was signal averaged for 1024 scans. Micro-Raman spectra were collected using a commercial, Thermo Scientific DXR Raman Microscope using a 10 mW, 532 nm laser line focused onto the sample surface using a 100 $\times$ , 0.9 NA objective. The signals were collected in confocal mode using a 25  $\mu\text{m}$  pinhole and an acquisition time of 5 s.

**Electromagnetic Modeling.** In order to take into account all the effects involved in these deeply subwavelength highly dispersive nanostructures, full-wave 3D electrodynamic calculations using the RF module of the finite-element package COMSOL were performed. The SiC optical constants were determined from ellipsometry and reflectance data obtained from the sample used and the geometric dimensions determined from SEM images. While the optical response of 6H–SiC is anisotropic, that is, the permittivity is different when light is polarized parallel or perpendicular to the basal plane, the derived optical constants demonstrated that this provided only a minor perturbation to the resultant resonant response and thus for simplicity were not included in the calculations. In an effort to closely match the experimental conditions, the simulations were undertaken using the incident optical field at 25 $^\circ$  to match that of the 15 $\times$  Cassegrain objective (0.58 NA) on the FTIR microscope. For the simulations, p-polarization was employed as it provides access to both transverse and longitudinal components of the electric field relative to the pillars within a single simulation. We also used normal incidence and compared that with the 25 $^\circ$  polarization simulation results to identify the features of the spectra exhibiting transverse and longitudinal components.

## ■ ASSOCIATED CONTENT

### 📄 Supporting Information

Reflection spectra detailing the influence of the reactive ion etching and subsequent hydrogen etching process upon the localized surface phonon polariton resonance linewidths and those illustrating the Fano-like interference effect between the LO phonon absorption with the monopolar SPhP resonance are provided. Further simulations from COMSOL illustrating the role of the angle of the incident electromagnetic field in coupling to the monopolar resonance and modifying the spatial profile of the transverse dipolar resonance are also presented. This material is available free of charge via the Internet at <http://pubs.acs.org>.

## AUTHOR INFORMATION

### Corresponding Author

\*E-mail: joshua.caldwell@nrl.navy.mil.

### Present Address

<sup>||</sup>(N.S.) NREIP Summer Student at NRL from University of California – Irvine; (F.J.B.) ASEE Postdoctoral Fellow (residing at NRL, Washington, DC).

### Author Contributions

The manuscript was written through contributions of all authors. All authors have given approval to the final version of the manuscript.

### Notes

The authors declare no competing financial interest.

## ACKNOWLEDGMENTS

The authors would like to thank Dr. Kathy Wahl, Dr. Dan Barlow, and Dr. Dan Burden of the Chemistry Division at the NRL for the use of their FTIR microscope and their assistance with the experimental setup. We would also like to thank Mr. Alex Boosalis of the University of Nebraska for his IR-VASE ellipsometry measurements from which initial optical constants of the SiC materials available at NRL were derived. We would also like to thank Dr. Lucas Lindsay and Dr. Thomas Reinecke for calculations of optical phonon lifetimes within SiC nanostructures used in the development of this effort and Professor Gennady Shvets for discussion of modal descriptions. Finally, electron beam lithography was performed at the NIST Center for Nanoscale Science and Technology. Funding for NRL authors was provided by the NRL Nanoscience Institute. F.J.B. acknowledges support from the ASEE-NRL Postdoctoral Fellowship Program. Y.F., S.M., and V.G. acknowledge support from EPSRC and Leverhulme Trust.

## REFERENCES

- Ritchie, R. H. *Phys. Rev. Lett.* **1957**, *106*, 874–881.
- Ozby, E. *Science (Washington, DC, United States)* **2006**, *311*, 189–193.
- Engheta, N. Taming Light at the Nanoscale. *PhyW* **2010**, *Sept*, 31–34.
- Veselago, V. G. *Phys.-Usp* **1967**, *10*, 509–514.
- Engheta, N.; Ziolkowski, R. W. *Metamaterials: Physics and Engineering Explorations*; Wiley & Sons: Hoboken, NJ, 2006.
- Kneipp, K.; Kneipp, H.; Kneipp, J. *Acc. Chem. Res.* **2006**, *39*, 443.
- Anderson, M. S. *Appl. Phys. Lett.* **2003**, *83*, 2964–2966.
- Aravind, P. K.; Metiu, H. *Surf. Sci.* **1983**, *124*, 506–5228.
- Osawa, M. *Surface-enhanced infrared absorption*; Springer-Verlag Berlin: Berlin, Germany, 2001; Vol. 81, pp 163–187.
- Khurgin, J. B.; Sun, G. *Appl. Phys. Lett.* **2011**, *99*, 211106.
- Boltasseva, A.; Atwater, H. A. *Science (Washington, DC, United States)* **2011**, *331*, 290–291.
- Khurgin, J. B.; Sun, G. *Appl. Phys. Lett.* **2010**, *96*, 181102.
- West, P. R.; Ishii, S.; Naik, G. V.; Emani, N. K.; Shalaev, V. M.; Boltasseva, A. *Laser Photon. Rev.* **2010**, *4*, 795–808.
- Maier, S. A. *Nat. Phys.* **2012**, *8*, 581–582.
- Grigorenko, A. N.; Polini, M.; Novoselov, K. S. *Nat. Photonics* **2012**, *6*, 749–758.
- Chen, J. N.; Badioli, M.; Alonso-Gonzalez, P.; Thongrattanasiri, S.; Hath, F.; Osmond, J.; Spasenoric, M.; Centeno, A.; Pesquera, A.; Godignon, P.; Elorza, A. Z.; Camara, N.; de Abajo, F. J. G.; Hillenbrand, R.; Koppens, F. H. L. Optical nano-imaging of gate tunable graphene plasmons. *Nature* **2012**, *487* (7405), 77–81.
- Hillenbrand, R.; Taubner, T.; Keilmann, F. *Nature* **2002**, *418*, 159–162.
- Ng, S. S.; Hassan, Z.; Abu Hassan, H. *Appl. Phys. Lett.* **2007**, *90*, 081902.
- Holmstrom, S. A.; Stievater, T. H.; Pruessner, M. W.; Park, D.; Rabinovich, W. S.; Khurgin, J. B.; Richardson, C. J. K.; Kanakaraju, S.; Calhoun, L. C.; Ghodssi, R. *Phys. Rev. B* **2012**, *86*, 165120.
- Dahan, N.; Niv, A.; Biener, G.; Kleiner, V.; Hasman, E. *Appl. Phys. Lett.* **2005**, *86*, 191102.
- Hafeli, A. K.; Rephaeli, E.; Fan, S. H.; Cahill, D. G.; Tiwald, T. E. *J. Appl. Phys.* **2011**, *110*, 043517.
- Bohren, C. F.; and Huffman, D. R. *Absorption and Scattering of Light by Small Particles*. In Ed.; John Wiley & Sons, Inc.: Weinheim, Germany, 2004; Vol. p 331–344.
- Mutschke, H.; Anderson, A. C.; Clement, D.; Henning, T.; Peiter, G. *Astron. Astrophys.* **1999**, *345*, 187–202.
- Schuller, J. A.; Taubner, T.; Brongersma, M. L. *Nat. Photonics* **2009**, *3*, 658–661.
- Taubner, T.; Korobkin, D.; Urzhumov, Y.; Shvets, G.; Hillenbrand, R. *Science (Wash.)* **2006**, *313*, 1595.
- Huber, A.; Ocelic, N.; Kazantsev, D.; Hillenbrand, R. *Appl. Phys. Lett.* **2005**, *87*, 081103.
- Le Gall, J.; Olivier, M.; Greffet, J.-J. *PhRvB* **1997**, *55*, 10105–10114.
- Huber, A. J.; Deutsch, B.; Novotny, L.; Hillenbrand, R. *Appl. Phys. Lett.* **2008**, *92*, 203104.
- Urzhumov, Y.; Korobkin, D.; Neuner, B.; Zorman, C.; Shvets, G. *J. Opt. A: Pure Appl. Opt.* **2007**, *9*, S322–S333.
- Greffet, J.-J.; Carminati, R.; Joulain, K.; Mulet, J. P.; Mainguy, S. P.; Chen, Y. *Nature* **2002**, *416*, 61–64.
- Neuner, B.; Wu, C.; Eyck, G. T.; Sinclair, M.; Brener, I.; Shvets, G. *Appl. Phys. Lett.* **2013**, *102*, 211111.
- Caldwell, J. D.; Stahlbush, R. E.; Mahadik, N. A. *J. Electrochem. Soc.* **2012**, *159*, R46–R51.
- Skowronski, M.; Ha, S. J. *Appl. Phys.* **2006**, *99*, 011101.
- Schuller, J. A.; Zia, R.; Taubner, T.; Brongersma, M. L. *Phys. Rev. Lett.* **2007**, *99*, 107401.
- Ameen, M.; Garcia-Etxarri, A.; Schnell, M.; Hillenbrand, R.; Aizpurua, J. *Chin. Sci. Bull.* **2010**, *55*, 2625–2628.
- Rockstuhl, C.; Salt, M. G.; Herzig, H. P. *J. Opt. Soc. Am. B: Opt. Phys.* **2005**, *22*, 481–487.
- Ocelic, N.; Hillenbrand, R. *Nat. Mater.* **2004**, *3*, 606–609.
- Businaro, L.; Limaj, O.; Giliberti, V.; Ortolani, M.; Di Gaspere, A.; Genci, G.; Ciasca, G.; Gerardino, A.; de Ninno, A.; Lupi, S. *Microelectron. Eng.* **2012**, *97*, 197–200.
- Chen, K.-P.; Drachev, V. P.; Borneman, J. D.; Kildishev, A. V.; Shalaev, V. M. *Nano Lett.* **2010**, *10*, 916–922.
- Collin, S.; Vincent, G.; Haidar, R.; Bardou, N.; Rommeluere, S.; Pelouard, J.-L. *Phys. Rev. Lett.* **2010**, *104*, 027401.
- Lee, S. H.; Johnson, T. W.; Lindquist, N. C.; Im, H.; Norris, D. J.; Oh, S.-H. *Adv. Funct. Mater.* **2012**, *22*, 4439–4446.
- Simpkins, B. S.; Long, J. P.; Glembocki, O. J.; Guo, J.; Caldwell, J. D.; Owrutsky, J. C. *Opt. Express* **2012**, *20*, 27725–27739.
- Zhu, X. L.; Ma, Y.; Zhang, J. S.; Xu, J.; Wu, X. F.; Zhang, Y.; Han, X. B.; Fu, Q.; Liao, Z. M.; Chen, L.; Yu, D. P. *Phys. Rev. Lett.* **2010**, *105*, 127402.
- Greffet, J.-J.; et al. *Nature* **2002**, *416*, 61–64.
- Koenderink, A. F. *Opt. Lett.* **2010**, *35*, 4208–4210.
- Silveirinha, M. G.; Engheta, N. *Phys. Rev. Lett.* **2006**, *97*, 157403.
- Sun, Y.; Edwards, B.; Alu, A.; Engheta, N. *Nat. Mater.* **2012**, *11*, 208–212.
- Nakashima, S.-i.; Harima, H. *Phys. Status Solidi A* **1997**, *162*, 39.
- Adato, R.; Yanik, A. A.; Amsden, J. J.; Kaplan, D. L.; Omenetto, F. G.; Hong, M. K.; Erramilli, S.; Altug, H. *Proc. Natl. Acad. Sci. U.S.A.* **2009**, *106*, 19227–19232.
- Taminiau, T. H.; Segerink, F. B.; van Hulst, N. F. *IEEE Trans. Antennas Propag.* **2007**, *55*, 3010–3017.
- Cetin, A. E.; Yanik, A. A.; Yilmaz, C.; Somu, S.; Busnaina, A.; Altug, H. *Appl. Phys. Lett.* **2011**, *98*, 111110.
- Wang, T.; Li, P.; Hauer, B.; Taubner, T. *Nano Lett.* **2013**, submitted for publication.

- (53) Maier, S. A. *Opt. Express* **2006**, *14*, 1957–1964.
- (54) Kuttge, M.; Garcia de Abajo, F. J.; Polman, A. *Nano Lett.* **2010**, *10*, 1537–1541.
- (55) Song, Y.; Wang, J.; Yan, M.; Qui, M. *J. Opt.* **2011**, *13*, 075001.
- (56) Fano, U. *PhRv* **1961**, *124*, 1866–1878.
- (57) Dhara, S.; Sahoo, P.; Tyagi, A. K.; Raj, B. *Surface Optical Mode in Semiconductor Nanowires*; InTech: Rijeka, Croatia, 2011; pp 3–26.
- (58) Wells, S. M.; Merkulov, I. A.; Kravchenko, I. I.; Lavrik, N. V.; Sepaniak, M. J. *ACS Nano* **2012**, *6*, 2948–2959.
- (59) Caldwell, J. D.; Glembocki, O. J.; Bezares, F. J.; Bassim, N. D.; Rendell, R. W.; Feygelson, M.; Ukaegbu, M.; Kasica, R.; Shirey, L.; Hosten, C. *ACS Nano* **2011**, *5*, 4046–4055.